Form-finding of Tessellated Tensegrity Structures

Keyao Song, Fabrizio Scarpa, Mark Schenk

Abstract

Many large-scale tensegrity structures are formed by assembling repeating units; a tensegrity tower formed by stacking tensegrity prisms is one example. Tessellated tensegrity structures tend to feature a repeating topology, but the geometry and self-stress vary across the assembly. In this work we design tensegrity structures by imposing periodic boundary conditions on a single unit cell to enforce repetitive topology, geometry and self-stress. A tessellated tensegrity tower is designed by using a stiffness matrix form-finding technique in combination with nodal position constraints. Since the tessellated tensegrity is not globally in equilibrium, a transition structure is required to balance the tessellated tensegrity tower on one side and to connect to a fixed boundary on the other. The challenge in designing the transition structure is that both coordinates and residual forces are simultaneously predefined at specific nodes. In this paper, we propose an adapted stiffness form-finding method to design the transition structure as an alternative method to the conventional ground structure method.

Keywords— tessellated tensegrity structures, form-finding method, transition structure, structural design

1 Introduction

A tensegrity is a prestressed pin-jointed truss structure, with struts under compression and cable members withstanding tension. Tensegrity structures offer the potential for lightweight design with a high strength-to-weight ratio; example applications include structural engineering and spacecraft design, as well as actuators [1] and architectural domes [2].

Form-finding is the process of identifying a self-equilibrated tensegrity configuration or an equilibrated tensegrity system [2, 3, 4, 5, 6, 7], which involves solving its nonlinear equilibrium equations. Form-finding methods can be broadly categorised into analytical and numerical techniques [8, 9, 10]. The former are particularly suited for tensegrities with limited number of members and structures with symmetry conditions [11, 12, 13, 14, 15, 16, 17]. Numerical methods are more generally applicable [18, 19, 20, 21, 22], and may include methods based on non-linear programming [23, 24, 25] and dynamic relaxation [26]. Force density form-finding methods constitute one of the leading numerical techniques. Schek [27] was the first to develop a force density form-finding method that solves the final configuration through linearising the equilibrium equations. Tran and Lee later used matrix decomposition of the force density matrix to find self-equilibrated tensegrity configurations [19]. As an alternative approach to force-density methods, Zhang et al. adopted a stiffness matrix form-finding method to design tensegrity structures in self-equilibrium [28].

The majority of works published on tensegrity form-finding methods focus on self-equilibrated tensegrity structures, as opposed to tensegrity structures under applied forces or imposed boundary conditions. Ground structure methods are often used for designing tensegrity structures with predefined nodal coordinates and external loads. Such methods identify a feasible topology (*i.e.* connectivity and cable/strut assignment) that meets the constraints and equilibrium equations [29]. Different approaches have been taken to set up the Mixed Integer Linear Problem (MILP) formulation of the ground structures methods, including minimising the total length of the members [30, 31], minimising material volume [32] or maximising member forces [33, 34].

This approach contrasts with other form-finding methods which assume a topology and find an equilibrated configuration, assuming an assignment of member force densities or material properties. As the final equilibrated configuration is unknown, it would be challenging for such form-finding approaches to impose conditions such as nodal coordinates and external loads *a priori*. In this paper, an adapted stiffness matrix form-finding method is proposed to maintain the versatile properties from that form-finding method, as well as to inherit the advantages from the ground structure method, where both residual forces and coordinates of nodes are predefined.

Several examples of large-scale tensegrity structures are formed by assembling basic units [1, 34, 35, 36, 37]. Masic et al. [38] design large-scale tensegrities by applying constraints involving specific heights or other shape parameters to tensegrity towers, but the resulting tensegrity plate may not be fully tessellated. Tran and Lee [39, 40] used a matrix decomposition method to find tensegrity plate-like structures in self-equilibrium; however, the double-layered repetitive tensegrity configuration is formed as a whole, rather than by tessellating repetitive units. Zhang et al. used affine transformations of a self-equilibrated tensegrity prism to build large scale tensegrity structure assemblies [41, 35]. Liu and Paulino [34] have designed tensegrity units in self-equilibrium by using the ground structure method to form assembled large-scale tensegrity metamaterials.

To illustrate the rationale for our work, we consider the tubular tensegrity structure in Figure 1. The topology graph shows the connectivity of the tensegrity members; note that this is a Class-I tensegrity as no more than one strut (*i.e.* compression member) connects at each vertex [42]. The structure has $n = 4$ identical repeating units along the circumferential direction. The structure (here referred to as a Tn tensegrity tower) has repeating odd/even layers along the axial direction. If we consider the self-equilibrated configuration, each compressive member within a layer will have the same force density (*i.e.* tension over length) due to the rotational symmetry; however, its magnitude varies along the length of the tubular structure. This example illustrates that, despite the repeating topology (say, between layers 2 and 4), the geometry and self-stress are different. Finite-layered tensegrity towers described in open liter-

ature (*e.g.* [43]) do not therefore consist of identical repeating unit cells, unless they are assembled from individually self-equilibrated modules. This variation of geometry and self-stress along a tessellated tensegrity structure has also implications for the manufacturing of these lattice configurations.

The question then arises how to design a truly repetitive tensegrity structure. A potential benefit of a purely periodic tessellation would be its ease of manufacture, as each unit cell consists of identical members and levels of self-stress. In this paper, we extend a stiffness matrix form-finding method with translational and rotational boundary conditions to design fully tessellated tensegrity structures, *i.e.* tubular tensegrity (1D tessellation) and tensegrity plates (2D tessellation). Unlike the tessellated unit case designed by Liu and Paulino [34] our tessellated units are not self-equilibrated, but are balanced by its adjoining elements. As a result, a tensegrity structure with a finite number of tessellated units will not be globally self-equilibrated. In order to connect such a structure to a boundary, a transition structure is designed to balance the tessellated tensegrity structure on one side, while connecting to a fixed boundary on the other. The main challenge during the form-finding process is represented by the need to specify simultaneously both coordinates and residual forces at the docking nodes (*i.e.*, the nodes on the transition structure that connect to the tessellated tensegrity). The ground structure method is traditionally used for such designs [34, 33]. In this paper, a novel adapted stiffness matrix form-finding method is proposed to address such design problems, and which can explore a larger geometric design space compared to the fixed nodal coordinates in a ground structure method.

The paper is organised as follows. Section 2 introduces the fundamental formulations of tensegrity structures, such as equilibrium, stiffness and stability. The stiffness matrix form-finding method for designing a repetitive tensegrity structure with position update constraints is then outlined in Section 3. The design process for a transition structure is described in Section 4, using a ground structure method as well as an adapted stiffness matrix form-finding method. Section 5 shows several examples of repetitive tensegrity structures, with related discussion presented in Section 6.

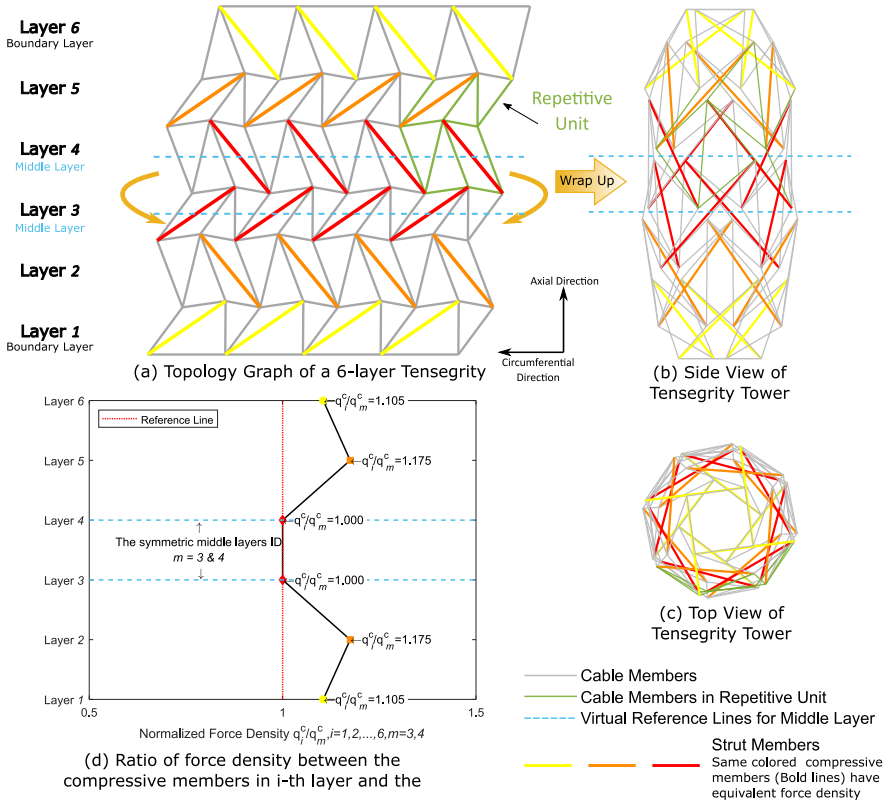

Figure 1: (a): Topology of a 6-layer *T4* tensegrity tower with repeating unit cell along the circumferential and axial directions. Same colour bold lines denote the compressive members (struts) with equivalent force density; thin lines denote the tensile members (cables). The force density of the compressive members is identical within each layer, but varies between layers. (b/c): side and top view of the self-equilibrated tensegrity tower. (d): normalised force density q_i^c/q_m^c of a compressive member in the i-th layer with respect to the middle layer m. The compressive members in each layer do not have the same force density, even when they are topologically identical.

2 Tensegrity Fundamentals

2.1 Connectivity and Force Density

Let us consider a tensegrity structure with n nodes and m members. The topology of the tensegrity is expressed through its connectivity or incidence matrix $\boldsymbol{C} \in \Re^{m \times n}$. If member k connects nodes i and j (with $i < j$), then the i-th and j-th elements of the k-th row of $\mathbf{C}$ are set as follows:

$$\mathbf{C}_{(kp)} = \begin{cases} 1 & \text{for } p = i \\ -1 & \text{for } p = j \\ 0 & \text{otherwise} \end{cases} \tag{1}$$

The nodal position vector $\mathbf{p} \in \Re^{n \times 3}$ contains all nodes with the i-th row indicating coordinates of the i-th node $\mathbf{p}_i = [x_i, y_i, z_i]$, where $\mathbf{x}, \mathbf{y}, \mathbf{z} \in \Re^{n \times 1}$ indicate the nodal position vector in the x, y and z direction. The k-th member element connecting nodes i and j is expressed as the k-th row of the projection vector of all members $\mathbf{e} \in \Re^{m \times 3}$. Those members can be expressed as:

$$\mathbf{e} = \mathbf{C}\mathbf{p} \tag{2}$$

The length of the k-th member l_k can be expressed as:

$$l_k = \|\mathbf{e}_k\| = \|\mathbf{p}_i - \mathbf{p}_j\| = \sqrt{(x_i - x_j)^2 + (y_i - y_j)^2 + (z_i - z_j)^2} \tag{3}$$

where $\| \cdot \|$ denotes the norm of the vector. The unit vector for the k-th element connecting nodes i and j is $\mathbf{e}_k^0 \in \Re^{1 \times 3}$:

$$\mathbf{e}_k^0 = \frac{\mathbf{e}_k}{l_k} \tag{4}$$

All members are here assumed to undergo linear elastic deformations. The internal

forces t_k of the k-th element can therefore be expressed as:

$$t_k = \begin{cases} 0 & \text{for a cable member } l_k \leq l_k^0 \\ g_k(l_k - l_k^0) & \text{otherwise} \end{cases} \tag{5}$$

where l_k, l_k^0 and g_k denote the length, the natural length and the axial stiffness of the element k. The axial stiffness g_k is expressed as:

$$g_k = \frac{E_k A_k}{l_k^0} \tag{6}$$

where E_k is the Young's modulus and A_k denotes the cross sectional area of the member k. In Section 3.2 the force density of the member q_k is used for the scaling of the strain for manufacturing feasibility of the tensegrity structures and q_k is defined as the tension over the length of the member, expressed as:

$$q_k = \frac{t_k}{l_k} = \frac{g_k(l_k - l_k^0)}{l_k} = \frac{E_k A_k}{l_k}\varepsilon \tag{7}$$

where ε is the engineering strain of the member. The strain energy of element $\mathbf{e}_k$ is denoted as:

$$U_k = \frac{1}{2} g_k (l_k - l_k^0)^2 \tag{8}$$

and is summed over all members to find the total strain energy of the structure.

2.2 Equilibrium Matrix

A tensegrity structure has an internal state of stress that is balanced against zero external forces (self-stress) and/or against applied loads. This equilibrium is described using the equilibrium matrix $\mathbf{A} \in \Re^{3n \times m}$:

$$\mathbf{A}\mathbf{t} = \mathbf{f}_{\text{ext}} \tag{9}$$

where $\mathbf{t} \in \Re^{m\times 1}$ is a vector of tensions, and $\mathbf{f}_{\text{ext}} \in \Re^{3n\times 1}$ is a vector of applied force components. The equilibrium matrix $\mathbf{A}$ for the entire structure is then expressed as:

$$\mathbf{A} = [\mathbf{a}_1, \mathbf{a}_2, \ldots, \mathbf{a}_m] \tag{10}$$

where the component $\mathbf{a}_k \in \Re^{3n\times 1}$ denotes the equilibrium matrix for the k-th member in the global coordinate system and it is defined so that the nodal forces $\mathbf{f}_k$ in equilibrium with a tension t_k in member k are given by:

$$\mathbf{a}_k[t_k] = \mathbf{f}_k \tag{11}$$

Hence, $\mathbf{a}_k$ has non-zero components corresponding to the nodes i and j connected to member k, and all other entries have zero components:

$$\mathbf{a}_k = \begin{bmatrix} \mathbf{a}_{k1} \\ \mathbf{a}_{k2} \\ \vdots \\ \mathbf{a}_{kn} \end{bmatrix}; \quad \begin{aligned} &\mathbf{a}_{ki} = \mathbf{e}_k^0 \\ &\mathbf{a}_{kj} = -\mathbf{e}_k^0 \\ &\mathbf{a}_{kl} = \mathbf{0}, \text{if } l \neq i \text{ and } l \neq j \end{aligned} \tag{12}$$

where $\mathbf{e}_k^0$ is unit vector of member k. Numerically, the p-th row of the equilibrium matrix $\mathbf{A}_{(p,:)}$ could be expressed as:

$$\mathbf{A}_{(p,:)} = \begin{cases} (\mathbf{C}^T\mathbf{\Lambda}_x)_{(i,:)} & \text{if } p = 3i-2 \\ (\mathbf{C}^T\mathbf{\Lambda}_y)_{(i,:)} & \text{if } p = 3i-1 \\ (\mathbf{C}^T\mathbf{\Lambda}_z)_{(i,:)} & \text{if } p = 3i \end{cases} \tag{13a}$$

where $i = 1, 2, \ldots, n$, and diagonal matrices:

$$\mathbf{\Lambda}_x = diag\left((\mathbf{Cx})_1/l_1, \ldots, (\mathbf{Cx})_m/l_m\right) \tag{13b}$$

$$\mathbf{\Lambda}_y = diag\left((\mathbf{Cy})_1/l_1, \ldots, (\mathbf{Cy})_m/l_m\right) \tag{13c}$$

$$\mathbf{\Lambda}_z = diag\left((\mathbf{Cz})_1/l_1, \ldots, (\mathbf{Cz})_m/l_m\right) \tag{13d}$$

where $\mathbf{Cx}$, $\mathbf{Cy}$ and $\mathbf{Cz} \in \Re^{m\times 1}$ are all column vectors, and $(\mathbf{Cx})_j$ denotes the j-th entry in the vector $\mathbf{Cx}$.

In this paper, we introduce a form finding method for tensegrity structures under external loads and imposed boundary conditions. The nodes are therefore divided into free nodes (*i.e.* free of constraints), docking nodes (*i.e.* with predefined coordinates and applied forces) and fixed nodes (*i.e.* fixed by the boundary conditions). The i-th column of connectivity matrix $\mathbf{C}$ represents the topology information of node i. Therefore, to derive the equilibrium matrix of fixed nodes and free nodes, the connectivity matrix can subsequently be partitioned as $\mathbf{C} = [\mathbf{C}_{\text{free}}\mathbf{C}_{\text{fix}}]$, where $\mathbf{C}_{\text{free}} \in \Re^{m\times n_{\text{free}}}$ and $\mathbf{C}_{\text{fix}} \in \Re^{m\times n_{\text{fix}}}$ are the connectivity matrices of the free and fixed nodes, and $\mathbf{C}_{\text{free}}(\mathbf{C}_{\text{fix}})$ is formed by selecting all columns relating to free (fixed) nodes from connectivity matrix $\mathbf{C}$. Here, n_{free} and n_{fix} are the number of free and fixed degrees of freedom, respectively. A tensegrity structure with n nodes has $3n$ degree of freedoms, and the structure can be constrained by placing boundary conditions on individual DOFs at a node. In this work, all DOFs at a node are fixed so that the dimension of the connectivity matrices of all degrees of freedom $\mathbf{C}_{\text{xfree}}$, $\mathbf{C}_{\text{yfree}}$ and $\mathbf{C}_{\text{zfree}}$ are the same; combined they form $\mathbf{C}_{\text{free}}$. The equilibrium matrix with the free nodes and under residual forces is updated and the p-th row of $\mathbf{A}_{\text{free}}$ numerically becomes:

$$(\mathbf{A}_{\text{free}})_{(p,:)} = \begin{cases} (\mathbf{C}_{\text{xfree}}^T \mathbf{\Lambda}_{\text{xfree}} + \mathbf{C}_{\text{xfree}}^T \mathbf{\Lambda}_{\text{xfix}})_{(i,:)} & \text{if } p = 3i-2 \\ (\mathbf{C}_{\text{yfree}}^T \mathbf{\Lambda}_{\text{yfree}} + \mathbf{C}_{\text{yfree}}^T \mathbf{\Lambda}_{\text{yfix}})_{(i,:)} & \text{if } p = 3i-1 \\ (\mathbf{C}_{\text{zfree}}^T \mathbf{\Lambda}_{\text{zfree}} + \mathbf{C}_{\text{zfree}}^T \mathbf{\Lambda}_{\text{zfix}})_{(i,:)} & \text{if } p = 3i \end{cases} \tag{14a}$$

where $i = 1, 2, \ldots, n_{free}$ and with diagonal matrics:

$$\mathbf{\Lambda}_{\text{xfree}} = diag((\mathbf{C}_{\text{xfree}}\,\mathbf{x}_{\text{free}})_1/l_1, \ldots, (\mathbf{C}_{\text{xfree}}\,\mathbf{x}_{\text{free}})_m/l_m) \tag{14b}$$

$$\mathbf{\Lambda}_{\text{xfix}} = diag((\mathbf{C}_{\text{xfix}}\,\mathbf{x}_{\text{fix}})_1/l_1, \ldots, (\mathbf{C}_{\text{xfix}}\,\mathbf{x}_{\text{fix}})_m/l_m) \tag{14c}$$

$$\mathbf{\Lambda}_{\text{yfree}} = diag((\mathbf{C}_{\text{yfree}}\,\mathbf{y}_{\text{free}})_1/l_1, \ldots, (\mathbf{C}_{\text{yfree}}\,\mathbf{y}_{\text{free}})_m/l_m) \tag{14d}$$

$$\mathbf{\Lambda}_{\text{yfix}} = diag((\mathbf{C}_{\text{yfix}}\,\mathbf{y}_{\text{fix}})_1/l_1, \ldots, (\mathbf{C}_{\text{yfix}}\,\mathbf{y}_{\text{fix}})_m/l_m) \tag{14e}$$

$$\mathbf{\Lambda}_{\text{zfree}} = diag((\mathbf{C}_{\text{zfree}}\,\mathbf{z}_{\text{free}})_1/l_1, \ldots, (\mathbf{C}_{\text{zfree}}\,\mathbf{z}_{\text{free}})_m/l_m) \tag{14f}$$

$$\mathbf{\Lambda}_{\text{zfix}} = diag((\mathbf{C}_{\text{zfix}}\,\mathbf{z}_{\text{fix}})_1/l_1, \ldots, (\mathbf{C}_{\text{zfix}}\,\mathbf{z}_{\text{fix}})_m/l_m) \tag{14g}$$

where $(\mathbf{C}_{\text{xfree}}\,\mathbf{x}_{\text{free}})_j$ and $(\mathbf{C}_{\text{xfix}}\,\mathbf{x}_{\text{fix}})_j$ denote the j-th entry in the vector $(\mathbf{C}_{\text{xfree}}\,\mathbf{x}_{\text{free}})$ and $(\mathbf{C}_{\text{xfix}}\,\mathbf{x}_{\text{fix}})$ respectively, for $j = 1, 2, \ldots, m$. The external force on the free nodes $\mathbf{f}_{\text{free,ext}}$ is then expressed as:

$$\mathbf{f}_{\text{free,ext}} = \mathbf{A}_{\text{free}}\,\mathbf{t} \tag{15}$$

The equilibrium matrix with boundary nodes can be derived in the same manner:

$$(\mathbf{A}_{\text{b}})_{(p,:)} = \begin{cases} (\mathbf{C}_{\text{xfix}}^T\,\mathbf{\Lambda}_{\text{xfree}} + \mathbf{C}_{\text{xfix}}^T\,\mathbf{\Lambda}_{\text{xfix}})_{(i,:)} & \text{if } p = 3i - 2 \\ (\mathbf{C}_{\text{yfix}}^T\,\mathbf{\Lambda}_{\text{yfree}} + \mathbf{C}_{\text{yfix}}^T\,\mathbf{\Lambda}_{\text{yfix}})_{(i,:)} & \text{if } p = 3i - 1 \\ (\mathbf{C}_{\text{zfix}}^T\,\mathbf{\Lambda}_{\text{zfree}} + \mathbf{C}_{\text{zfix}}^T\,\mathbf{\Lambda}_{\text{zfix}})_{(i,:)} & \text{if } p = 3i \end{cases} \tag{16}$$

where $i = 1, 2, \ldots, n_{fix}$. The boundary forces on the fixed nodes $\mathbf{f}_{\text{b,ext}}$ can then be calculated using the equilibrium matrix:

$$\mathbf{f}_{\text{b,ext}} = \mathbf{A}_{\text{b}}\,\mathbf{t} \tag{17}$$

At each iteration of the original SMFF method the unbalanced force (or residual force) at a node is calculated. The program stops when the unbalanced forces falls below a specified threshold (nominally 1×10^{-7} multiplied by the maximum tensions in the members, which here gives 1×10^{-3} N). The unbalanced force of each node is defined as the resulting force generated by the internal stresses of the members connected to the node. For equilibrium, the unbalanced force at a node has the same

magnitude and opposite direction of the applied external force or reaction force at fixed nodes. The way the unbalanced forces are calculated in the SMFF method [28] is, however, no longer valid when fixed boundary nodes are present and when the structure is subjected to external forces. The unbalanced forces are therefore derived through equilibrium equations. For a free node, the relationship between the unbalanced force $\mathbf{u}_{\text{free}}$ and the external force $\mathbf{f}_{\text{free,ext}}$ at each node is:

$$\mathbf{u}_{\text{free}} = -\mathbf{f}_{\text{free,ext}} \tag{18}$$

For a fixed node, the unbalanced force is forced to be zero as the fixed node is constrained during the form-finding process, thus:

$$\mathbf{u}_{\text{fixed}} = \mathbf{0} \tag{19}$$

The unbalanced force $\mathbf{u}_{\text{docking}}$ of the docking nodes belonging to the transition structure with applied forces $\mathbf{f}_{\text{docking}}$ is redefined as the difference between the residual forces $\mathbf{f}_{\text{free,ext}}$ and external load $\mathbf{f}_{\text{docking}}$, given as:

$$\mathbf{u}_{\text{docking}} = -(\mathbf{f}_{\text{free,ext}} - \mathbf{f}_{\text{docking}}) \tag{20}$$

The expression relating the unbalanced forces $\mathbf{u}$ in terms of the classes of nodes, with $\mathbf{t}$ as the tension vector of all members is as follows:

$$\mathbf{u} = \begin{cases} -(\mathbf{A}_{\text{free}}\,\mathbf{t} - \mathbf{f}_{\text{docking}}) & \text{for docking nodes} \\ -(\mathbf{A}_{\text{free}}\,\mathbf{t}) & \text{for free nodes} \\ \mathbf{0} & \text{for boundary nodes} \end{cases} \tag{21}$$

2.3 Stiffness Matrix and Stability

The tangent stiffness matrix $\boldsymbol{K} \in \Re^{3n\times 3n}$ of a self-equilibrated tensegrity structure is given by [44]:

$$\boldsymbol{K} = \mathbf{A}\,(\mathbf{G} - \mathbf{Q})\,\mathbf{A}^T + \mathbf{S} \otimes \mathbf{E} \tag{22}$$

where $\mathbf{A} \in \Re^{3n \times m}$ is the equilibrium matrix, and $\mathbf{G}$ and $\mathbf{Q} \in \Re^{m \times m}$ are diagonal matrices of element axial stiffness and element force density, respectively. The second part is formed from the Kronecker product ($\otimes$) of the stress matrix (or force density matrix) $\mathbf{S} \in \Re^{n \times n}$, which is expressed as:

$$\mathbf{S} = \mathbf{C}^T \mathbf{Q} \mathbf{C} \tag{23}$$

and the identity matrix $\mathbf{E} \in \Re^{d \times d}$, where d is dimension of the structure.

The tangent stiffness matrix of the tensegrity structure is instrumental in the selected form-finding method. Further, the stability of equilibrium configuration can be evaluated from the tangent stiffness matrix. If the tangent stiffness matrix is positive-definite (*i.e.*, the quadratic form of $\mathbf{K}$ is positive with respect to any non-trivial motion $\boldsymbol{d}$):

$$\mathbf{d}^T (\mathbf{K}) \mathbf{d} > 0 \tag{24}$$

then the structure is stable when its rigid body motions are constrained. Equivalently, the eigenvalues of the stiffness matrix $\mathbf{K}$ are real and positive apart from $d \times (d+1)/2$ zero eigenvalues corresponding to rigid body motions [45, 46].

For tensegrity structures under simultaneous applied loads and boundary conditions, the stiffness matrix $\mathbf{K}$ is modified into $\bar{\mathbf{K}}$, where all non-diagonal entries on the rows and columns which correspond to constrained DOFs are modified to 0 and the diagonal entries are modified to 1. The modified stiffness matrix must be positive definite to ensure the convergence of the form-finding calculation. A negative eigenvalue of $\bar{\mathbf{K}}$ indicates instability of the structure in the current iteration, whereas a zero eigenvalue might cause divergence of the numerical procedure. In order to proceed with the calculation process, the stiffness matrix $\bar{\mathbf{K}}$ is further modified into $\tilde{\mathbf{K}}$ by introducing a 'temporary stiffness' at some DOFs to ensure a positive definite stiffness matrix. The magnitudes of the temporary stiffness are determined by the lowest eigenvalue of $\bar{\mathbf{K}}$. After a few iterations, the stiffness matrix $\bar{\mathbf{K}}$ will become a positive definite matrix; thus $\tilde{\mathbf{K}} = \bar{\mathbf{K}}$ and no further modification will be needed. The details on constraining the stiffness matrix and adding temporary stiffness matrix are described in Section 3.

3 Form-Finding of Tessellated Tensegrities

The stiffness matrix form-finding method (SMFF method [28]) is able to find a self-equilibrated tensegrity structure for a given topology by seeding initial values associated with the geometry of the structure, and the natural lengths and axial stiffness of the members. A self-equilibrated solution is found by iteratively minimising the residual forces at the nodes by updating the nodal coordinates. As shown in this work, the stiffness matrix form-finding approach can be modified to satisfy different types of requirements, such as applying symmetry constraints to nodes and members of the tensegrity structure, or specify external applied loads.

Our objective is to design a tessellated tensegrity structure by form-finding a single unit cell with appropriate symmetry boundary conditions. As the unit cell relies on connectivity to adjacent units, this complicates the formulation of the tangent stiffness matrix required for the SMFF methodology. The solution for designing the tessellated tensegrity structures using a single unit cell is carried out by the 'Position Update Constraint' during the form finding iteration process. The calculation model is shown in Figure 2, where the nodes of the model are divided into two groups: independent nodes and dependent nodes. The nodal position of the dependent nodes depends on the position of the independent nodes by the conditions of rotational and translational symmetry. During the form finding iteration process, the dependent nodes are initially fixed, allowing a stiffness matrix to be formulated, and are updated after new positions for the independent nodes are found. This section outlines the adapted stiffness matrix form-finding method for tessellated tensegrity structures.

3.1 Position Update Constraints

The unit cell for form-finding a tessellated tensegrity tower structure is shown in Figure 2. The calculation model contains 19 members (4 strut and 15 cable members) and differs from the repetitive unit cell shown in Figure 3(b) in order to capture its connectivity to (and resulting forces from) adjacent nodes during the form-finding process. There exists a set of four *independent* nodes $I = [a, b, c, d]$, with a corresponding *de-*

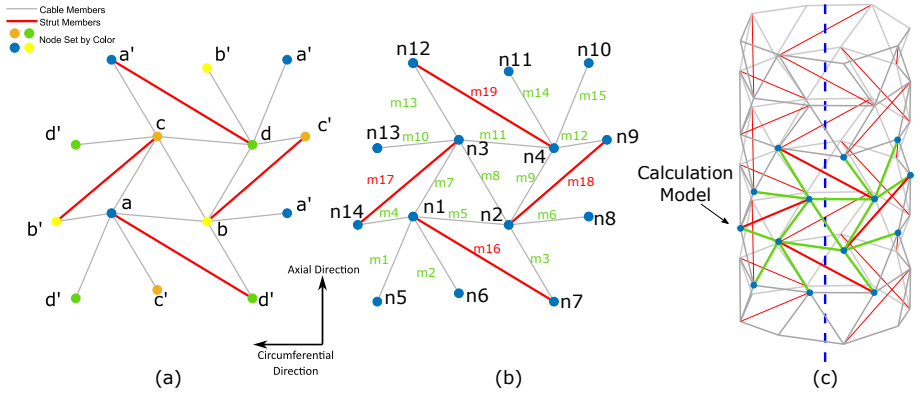

Figure 2: (a) Calculation model of the repetitive tensegrity tower structure unit. There are four independent nodes (a, b, c and d) denoted by four different colours. The dependent nodes are indicated as a', b', c' and d'. The dependent nodes are in rotationally symmetric or translational relative positions to the independent nodes. (b): The topology graph of the calculation model, nodes are labeled as $ni, i = 1, 2, \ldots, 14$, members are labeled as $mi, i = 1, 2, \ldots, 19$, where green font (red) represents cables (struts). (c): Placement of the calculation model in the global tessellated structure.

pendent node set $D = [a', b', c', d']$. The coordinates of dependent nodes are generated via rotational or translational transformations of the independent nodes.

The coordinates of dependent node i' $\mathbf{p}_{i'} \in \Re^{3\times 1}$ are determined from the coordinates $\mathbf{p}_i \in \Re^{3\times 1}$ of its corresponding independent node i as follows:

$$\mathbf{p}_{i'} = \mathbf{R}\mathbf{p}_i + \delta\mathbf{t} \tag{25}$$

using a rotation around the cylinder axis

$$\mathbf{R} = \begin{bmatrix} \cos(\theta) & \sin(\theta) & 0 \\ -\sin(\theta) & \cos(\theta) & 0 \\ 0 & 0 & 1 \end{bmatrix}$$

where $\theta = 2\pi/T_n$ and the T_n refers to the symmetry of the tensegrity prism, as well

as a translation $\delta\mathbf{t}$ along the cylinder axis, where

$$\delta = \begin{cases} 1 & \text{if } k' \text{ is a translational dependent node} \\ 0 & \text{if } k' \text{ is a rotational dependent node} \end{cases}$$

and $\mathbf{t} = [0, 0, z_{\text{trans}}]^T$. Using this approach, the coordinates of the dependent nodes are updated after each iteration of the SMFF method.

3.2 Form-Finding Process

The process to apply the SMFF method with constraints for nodal updates to design the tessellated tensegrity structures formed with repetitive units is as follows:

1. Provide a random initial position of the structure nodes $\mathbf{P}^0$. From the natural length l_k^0 and axial stiffness g_k of the members, calculate the initial strain energy U^0 and the stiffness matrix $\mathbf{K}^0$. The superscript denotes the N-th iteration step, with here $N = 0$ for first seed of coordinates.

2. Calculate the force density q^0 and the tensions t^0 of each member. Select all DOFs corresponding to the dependent nodes to be fixed and divide the connectivity matrix into $\mathbf{C}_{\text{free}}$ and $\mathbf{C}_{\text{fix}}$. The equilibrium matrix can therefore be expressed from Equation (13) and the unbalanced forces $\mathbf{u}^N$ are derived by equilibrium equation from Equation (21).

3. In order to prevent the rigid body motion of the structure, the fixed nodes constraints should be added by modifying the stiffness matrix $\mathbf{K}$ into $\bar{\mathbf{K}}$.

$$\bar{\mathbf{K}} = \begin{cases} \bar{\mathbf{K}}_{JJ} = 1 & \text{if the } J\text{-th DOF is constrained} \\ \bar{\mathbf{K}}_{LJ} = \bar{\mathbf{K}}_{JL} = 0 & \text{if the } J\text{-th } (J \neq L) \text{ DOF is constrained} \\ \bar{\mathbf{K}}_{LJ} = \mathbf{K}_{LJ} & \text{otherwise} \end{cases} \tag{26}$$

   where $J, L = 1, 2, 3, ..., 3n$. Since only the unbalanced forces of the free nodes are considered, the influence of the fixed nodes is eliminated by zeroing those forces; hence we modify $\mathbf{u}^N$ into $\bar{\mathbf{u}}^N$ by adding the fixed nodes constraints to

the i-th entry:

$$(\bar{\mathbf{u}})_i = \begin{cases} 0 & \text{if } i\text{-th DOF is constrained} \\ \mathbf{u}_i & \text{otherwise} \end{cases} \tag{27}$$

where $i = 1, 2, \ldots, 3n$. If the stiffness matrix $\bar{\mathbf{K}}$ is not positive definite, modify the same matrix by implementing the following criteria:

$$\tilde{\mathbf{K}} = \begin{cases} \bar{\mathbf{K}} & \text{if } K \text{ is positive definite} \\ \bar{\mathbf{K}} + \xi |\lambda_{\bar{\mathbf{K}},\min}| \, \mathbf{E}^{3n} & \text{otherwise} \end{cases} \tag{28}$$

where $\mathbf{E}^{3n} \in \Re^{3n \times 3n}$ is the identity matrix, $\lambda_{\bar{K},min}$ is the minimum eigenvalue of the $\bar{K}$ with $|\lambda_{\bar{K},min}|$ denoting its absolute value, $\xi = 1.01$ is a coefficient. Combined with the unbalanced forces from Equation (21), the independent nodes in the calculation model are corresponding free nodes and this is expressed as:

$$\bar{\mathbf{u}}^N = \begin{cases} -(\mathbf{A}_{\text{free}} \mathbf{t}^N) & \text{for independent (free) nodes} \\ 0 & \text{for dependent (fixed) nodes} \end{cases} \tag{29}$$

4. Calculate the increment of the displacements of the independent nodes DOFs:

$$\Delta \mathbf{P}^N = (\tilde{\mathbf{K}}^{N-1})^{-1} \, \bar{\mathbf{u}}^{N-1}$$

5. Add the increment of the displacements onto the previous displacements:

$$\mathbf{P}^N = \mathbf{P}^{N-1} + (\eta^N) \, \Delta \mathbf{P}^N$$

The range of coefficients for the displacements increments is constant and is denoted as $\eta \in (0, 1]$. At each iteration step and after calculating $\mathbf{P}^N$, the value of η is the largest number that minimises the strain energy of the structure. First, we assign $\eta = 1$ to be the coefficient value and update the nodal coordinate and calculate the strain energy. If the strain energy decreases compared to the one in the previous step, $\eta = 1$ is used in the current step; otherwise, the

bisection method is employed to find the maximum value $0 < \eta_{\max} < 1$ that can decrease the strain energy.

6. Update the coordinates of the dependent nodes due to the symmetry or translation conditions using Equation (25) as described in Section 3.1.

7. Iterate the procedure until the unbalanced forces on independent free nodes is lower than or equal to a specific threshold value u_{th}: $\bar{\mathbf{u}}_i \leq u_{th}$, for $i = 1, 2, \ldots, 3n$

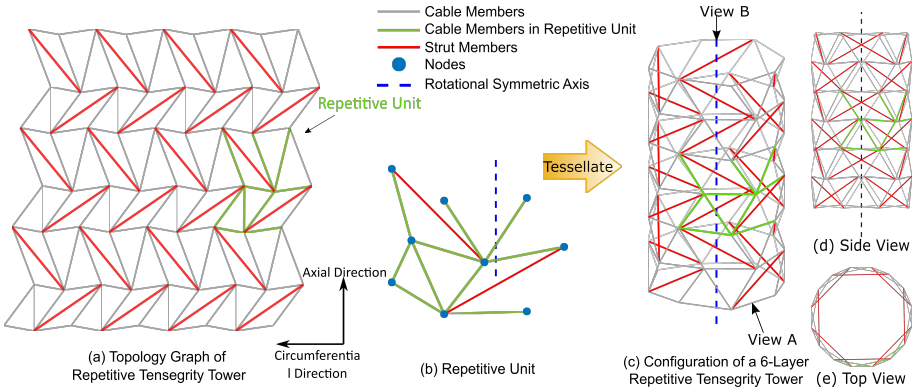

Figure 3: (a): The topology graph of a 6-layer T_4 tessellated tensegrity tower. One of repetitive units is highlighted. (b): 3D view of the repetitive unit with the rotational axis. The repetitive unit cell consists of 9 nodes (4 independent and 5 dependent) and 12 members (10 tensile and 2 compressive). (c): By rotating the repetitive unit about the axis, a rotationally-symmetric layer is formed, which is translated axially to form a repetitive tensegrity tower. (d/e) side and top views of of the repetitive tensegrity tower.

Results: Tensegrity Tower The outcome of the design process for the T_4 tessellated tubular tensegrity structure is shown in Figure 3; the connectivity matrix of the calculation is shown in Appendix A.1. Results for T_3 and T_5 tensegrity structures are shown in Section 5. Initial length l_k^0, axial stiffness g_k and cross-sectional area A_k for each of the members in calculation model are listed in Table 1, alongside calculated axial strain and tension coefficient. All members are assumed linear-elastic and have Young's modulus $E = 210$ GPa. The bars are assumed not buckle, but the self-stress in the structure is scaled such that no members exceed 0.2% strain; this informs the

selection of the adjustment coefficient c_1 in Equation 30b. The final nodal coordinates are listed Table 2.

It should be noted that the repetitive unit cell is equilibrated by the presence of adjacent repetitive unit cells in both circumferential and axial directions. Therefore, the 6-layer tessellated tubular tensegrity shown in Figure 3(c) is imbalanced as the ends of the tessellated tensegrity are not equilibrated. Therefore so-called transition structures (also referred to as 'end caps') are necessary to connect the tensegrity to a fixed boundary to provide overall structural equilibrium. Further, the stability of the tessellated structure cannot readily be assessed as it is currently not in equilibrium; therefore a transition structure must be designed first.

	(mm)	(N/mm)	(mm^2)	%	(N/mm)
Member ID k	l_k^0	g_k	A_k	ε_k	q_k
1, 8, 15	175	339	0.283	0.169	0.572
2, 3, 7, 9, 13, 14	162	366	0.283	0.289	1.058
4, 5, 6, 10, 11, 12	180	329	0.283	0.097	0.319
16, 17, 18, 19	300	54977	78.54	-0.001	-0.634

Table 1: Member properties in T_4 calculation model

	(mm)	(°)	(mm)
Node ID i	r_i	θ_i	z_i
1	234.634	0	149.175
2	234.634	45	134.566
3	234.634	22.372	283.742
4	234.634	67.372	269.133
5	234.634	227.372	0.000
6	234.634	22.372	14.609
7	234.634	67.372	0.000
8	234.634	90	149.175
9	234.634	112.372	283.742
10	234.634	90	418.308
11	234.634	45	403.699
12	234.634	0	418.308
13	234.634	227.32	269.133
14	234.634	315	134.566

Table 2: Nodal coordinates for final configuration for T_4 calculation model

In order to evaluate structures that are physically realisable, the member strains are

adjusted while maintaining the equilibrated state [38]. Two approaches are considered, which both keep the Young's modulus and cross section area of the member unchanged. The first method scales the coordinates of the structure while keeping the force density unchanged (*i.e.* an affine transformation); the second method scales the force density without scaling the structure. In this paper, the latter method is used as it adjusts the strain in a more precise way while maintaining the dimensions of the structure. From Equation 7, the force density is linked to the strain of the member. After the adjustment, the new strain $\varepsilon' = c_1\varepsilon$, then $q'_k = c_1 q_k$. The final length of each member l_k is unchanged as the coordinates are unchanged, so the adjusted natural length of member is expressed as:

$$\frac{(l_k - l_k^{0'})}{l_k^{0'}} = c_1 \frac{(l_k - l_k^0)}{l_k^0} \tag{30a}$$

$$l_k^{0'} = \frac{(l_k l_k^0)}{c_1 l_k + (1 - c_1) l_k^0} \tag{30b}$$

The maximum calculated strain of 0.289% is too high for conventional metallic materials. Assuming a yield strain of 0.2%, we assign $c_1 = 0.5$, and the final results are listed in Table 3. The range of the scaling coefficient c_1 is determined by ratio of the highest strain ϵ_{max} in member to the yield boundary of 0.2%, which is $(0, \frac{0.2\%}{\epsilon_{max}})$.

	(mm)	(N/mm)	(mm^2)	%	(N/mm)
Member ID k	$l_k^{0'}$	g_k	A_k	ε'_k	q'_k
1, 8, 15	175	339	0.283	0.0844	0.0286
2, 3, 7, 9, 13, 14	162	366	0.283	0.145	0.529
4, 5, 6, 10, 11, 12	180	330	0.283	0.0484	0.160
16, 17, 18, 19	300	54978	78.54	-0.000577	-0.317

Table 3: Member properties in T_4 calculation model after strain adjustment

4 Design of Transition Structures

The tessellated tensegrity structure designed in the previous section is not globally self-equilibrated as each unit cell depends on connecting members for equilibrium. The purpose of a transition structure is to balance a tessellated tensegrity tower on one side and connect to a fixed boundary on the other side. There are three sets of

nodes within the transition structure: the boundary nodes that connect to the external environment, the docking nodes that balance the tessellated tensegrity tower, and the remaining nodes that are free from constraints.

The form finding challenge is that both residual forces and nodal coordinates are simultaneously predefined for the docking nodes; see Figure 4. Further, the Class-I constraint of the overall assembly is imposed during the design process. Two alternative and complementary form-finding methods are utilised to design transition structures for the tessellated tensegrity towers: (i) an adapted ground structure method with symmetry constraints; (ii) an extension of the stiffness-matrix form-finding method to incorporate external loads.

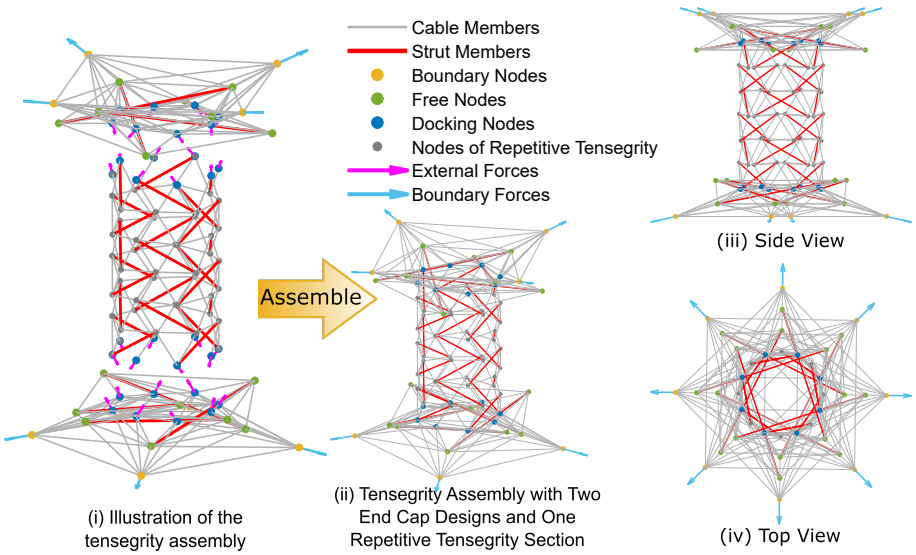

Figure 4: (i): Two transition structures connect to each end of the tessellated tensegrity structure. The blue arrows denote the residual forces on the boundary, while magenta arrows indicate the external forces on the docking nodes. The external forces on the repetitive tensegrity tower (middle part) are balanced by the transition structures on the top and the bottom after assembly. (ii): Overview of the assembly; the tensegrity tower with repetitive units is balanced by the transition structures on the top and bottom. (iii/iv): Side and top view of the assembly.

4.1 Ground Structure Method

The ground structure form finding approach is also known as topology optimization in the design of tensegrity structures [31]. In these methods, the nodal positions of the final configuration as well as the external loads are prescribed, and the topology (*i.e.* connectivity and cable/strut assignment) of the structure is determined. The initial ground structure consists of a full connectivity between all nodes, and the form-finding process identifies which members can be removed to give a resulting structure that meets the nodal position and external loading conditions. As a result, the ground structure method represents a promising tool to identify the configuration of the transition structures for the tessellated tensegrity tower. In this paper we adapt the ground structure formulation proposed by Liu et al. [33] and expand its capabilities by including external loads and applying symmetry and Class-I connectivity constraints.

The ground structure form-finding method can be formulated as a Mixed Integer Linear Programming (MILP) problem [30, 31] with the objective of maximising the tension in the cable members [33]:

$$\max_{\mathbf{s}',\mathbf{t}',\mathbf{c}'} \mathbf{1}^T(\mathbf{t}' - \mathbf{c}') \tag{31a}$$

subject to:

$$\mathbf{A}_{\text{free}}(\mathbf{t}' - \mathbf{c}') = \mathbf{f}_{\text{free,ext}} \tag{31b}$$

$$t'_k \geq 0 \tag{31c}$$

$$1 \geq s'_k \geq c'_k \geq 0 \tag{31d}$$

$$s'_k \in \mathbb{Z} \tag{31e}$$

$$\mathbf{G}_g\mathbf{s}' \leq \mathbf{1} \tag{31f}$$

$$\mathbf{Q}\begin{bmatrix}\mathbf{t}'\\ \mathbf{c}'\end{bmatrix} = \mathbf{0} \tag{31g}$$

which is solved by using the 'intlinprog' solver in MATLAB optimization toolbox [47]. The axial load of every member in a tensegrity ground structure with n_g nodes and

m_g members is represented by the difference between the tension $\mathbf{t}' \in \Re^{m_g \times 1}$ and the compression $\mathbf{c}' \in \Re^{m_g \times 1}$ in each member. We therefore obtain two non-negative variables by decoupling the tension and compression of the force density. The binary integer variable $\mathbf{s}' \in \Re^{m_g \times 1}$ determines the type of each member; $s'_k = 1$ indicates that the k-th member in the ground structure is a strut member; $s'_k = 0$ indicates a cable member, or that the member is deleted from the ground structure (if the final stress $t'_k - c'_k = 0, s'_k = 0$ for any member k) — deleted members are not shown in the final configuration. Inequality constraint Equations 31c and 31d provide bounds on variables $\mathbf{s}', \mathbf{t}', \mathbf{c}'$, and $\mathbb{Z}$ in Equation 31e represents the integer set.

Equilibrium under applied external loads $\mathbf{f}_{\text{free,ext}} \in \Re^{3n_{\text{free}}}$ is described by Equation 31b, where $\mathbf{A}_{\text{free}}$ denotes the equilibrium matrix of free nodes and fixed nodes as expressed in Equation (13).

The matrix $\mathbf{G}_g \in \Re^{n_g \times m_g}$ is the incidence matrix, which contains information about the topology of the structure and it is used to impose the Class-I tensegrity constraint. $\mathbf{G}_g$ is expressed as:

$$\mathbf{G}_{g,ik} = \begin{cases} 1 & \text{if node i is connected by member k} \\ 0 & \text{otherwise} \end{cases} \tag{32}$$

where $i = 1, 2, ..., n_g$ and $k = 1, 2, ..., m_g$. Changing the integer upper bound for Equation 31f will lead to a corresponding Class-X constraint. Note that the inequality means that individual nodes might have fewer compression members, or might even only have tensile members.

Equation 31g imposes the symmetry constraints on the elements in the ground structure using matrix $\mathbf{Q} \in \Re^{c_{all} \times 2m_g}$ whose rows represent all combinatorics of every two rotationally symmetric members in any independent symmetric groups where c_{all} denotes the number of combinations from the independent symmetry groups. Since the final stress of any member k is represented by the combination of two independent variables t_k and c_k, the symmetry conditions cannot be imposed on members directly. Therefore, one critical numerical step is to impose the symmetry constraint

on the tensile and compressive members separately. First, the rotationally symmetric members in the ground structure are identified by their spatial positions and placed into one independent symmetric member set; then symmetry conditions are imposed on strut members and cable members separately through constraining the variable c'_k (t'_k) for any strut (cable) member k. The process for building the $\mathbf{Q}$ matrix to impose symmetric constraints and to fit the formulations is as follows. Consider the m-th independent symmetric members set $I_m = [m_1, m_2, m_3, m_4]$ where m_i is the ID of the member, contains four members. For strut members, any randomly picked two members in the same symmetric members set should satisfy the equality:

$$c'_i - c'_j = 0, i \neq j, i, j \in I_m \tag{33}$$

from a combinatorics point of view, there are 6 (number of combinations for choosing any 2 from a 4 members set I_m) equalities. An identical formulation applies to the tension t_i for the cable members. Each row of the combinatorics matrix $\mathbf{Q}$ records one pair of equalities which correspond to the Equation 33 (equivalently for t_i), hence the expression for i-th row of $\mathbf{Q}_{(i,:)}$ representing one pair of equalities $t'_{m_1} - t'_{m_2}$ and $c'_{m_1} - c'_{m_2}$:

$$\mathbf{Q}_{(i,k)} = \begin{cases} 1 & \text{if } k = m_1, m_g + m_1 \\ -1 & \text{if } k = m_2, m_g + m_2 \end{cases} \tag{34}$$

so that the whole combinatorics matrix $\mathbf{Q} \in \Re^{c_{all} \times 2m_g}$ satisfies Equation 31g. For a ground structure with p independent symmetric member sets and m_{I_k} members in the k-th set I_k where $k = 1, 2, \ldots, p$, $c_{all} = \sum_{i=1}^{p} \frac{m_{I_i}!}{2!(m_{I_i}-2)!}$ and is calculated by 'n choose k formula' from the combinatorics.

Results The transition structures that connect to the T_4 tubular tessellated tensegrity are here designed to maintain the same rotational symmetry [48, 38]. Further, since half of the docking nodes from the tubular tessellated tensegrity present a connected strut member, the constraint Equation 31f should be rewritten to ensure that the final combination of transition structures and tessellated tubular tensegrity re-

mains a Class-I tensegrity. For any docking node in the transition structure with ID i and corresponding docking node in the tubular tessellated tensegrity that are not connected to a strut, the constraint should be rewritten as the i-th entry of the vector $\mathbf{G}_g\mathbf{s}'$:

$$(\mathbf{G}_g\mathbf{s}')_{(i)} \leq 0$$

The coordinates of the free nodes in the ground structure must be chosen such that an equilibrated solution can be found. Figure 5(c) illustrates the position of the docking, boundary and free nodes in the transition structure. The free node sets are placed at a radial, angular and axial offset from the docking nodes. This resulted in an initial ground structure with $n_g = 20$ nodes and $m_g = 172$ members (members whose center lies inside a central cylindrical restriction volume with radius of 10 mm are deleted). Further, the MATLAB solver requires both the upper/lower bounds of the variables, so instead of being infinite as suggested by Equation 31c, the tension is constrained in a way that maximum strain in the transition structure is 0.18%. The final transition structure for the tessellated tensegrity is shown in Figure 5 (and previously in Figure 4) and consists of $m_t = 96$ members. From the output of the MILP formulation, the member tension, member length, and topology are known. Using a Young's Modulus $E = 210$ GPa, a cross section area 0.283 mm^2 for cable members and 78.54 mm^2 for strut members, the natural length of each member could be calculated and all information for the structure is solved.

The main strengths of the ground structure method are that the topology is not needed as the initial information, and that the ability to change the upper bounds of the variables expands the design space for the final configuration. For example, the strain in the members can be constrained by setting up an upper bound for tension variables using Equation 7. However, one major limitation is represented by the fact that one might not select a set of coordinates for the ground structure that will lead to a feasible solution.

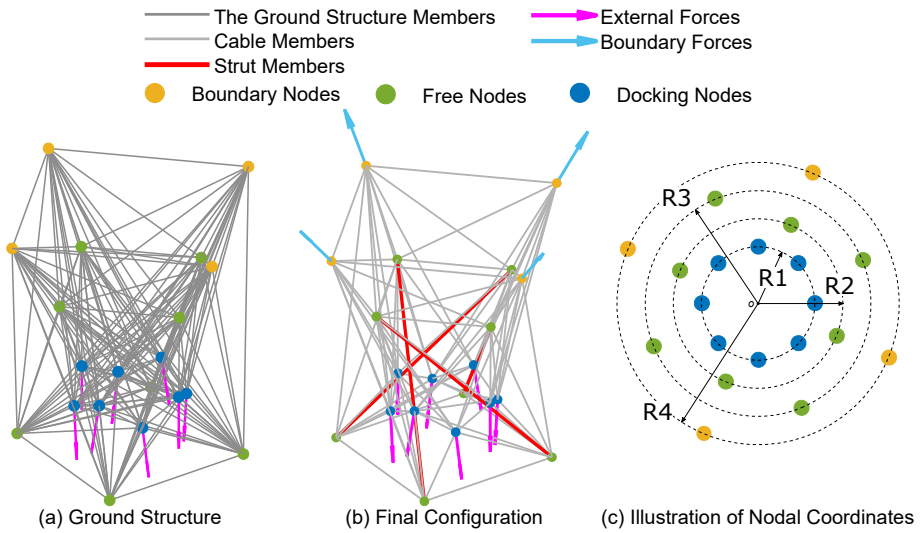

Figure 5: Ground structure methodology to design a transition structure. (a): The position and residual forces at the docking nodes (blue dots) are predefined, as well as the position of the boundary nodes (ochre dots). Free nodes (green dots) are selected at will. The initial ground structure is formed by finding all connections between nodes. (b): The final configuration of the form-finding process of the transition structure, which is in equilibrium with external loads and subject to symmetry and Class I assembly constraints. (c): Illustration of coordinates of the free nodes.

			(mm)	(°)	(mm)
Node ID i	Node Type	Radius ID	r_i	θ_i	z_i
1	docking node	R_1	234.634	0	50
2				90	
3				180	
4				270	
5	docking node	R_1	234.634	45	35.391
6				135	
7				225	
8				375	
9	free node	$R_2 = 1.5R_1$	351.951	67.372	130
10				157.372	
11				247.372	
12				337.372	
13	free node	$R_3 = 2R_1$	469.268	22.372	0
14				112.372	
15				202.372	
16				392.372	
17	fixed node	$R_4 = 2.5R_1$	586.685	67.372	200
18				157.372	
19				247.372	
20				337.372	

Table 4: Nodal coordinates of the ground structure/transition structure.

4.2 Adapted Stiffness Matrix Form-Finding Method

Since the ground structure method can only find a topology solution that fits the constraints with given nodal coordinates, it essentially limits the design space by providing only a discrete number of possibilities to solve the objective function and constraints. By comparison, the stiffness matrix form-finding method allows nodes to move freely during the form-finding process, albeit within a given topology, thereby increasing its potential to find an equilibrium configuration. In order to apply the stiffness matrix form-finding method to the design of transition structures it is here modified to incorporate the ability to simultaneously specify residual forces and coordinates at specific nodes (specifically, the docking nodes).

The process of the adapted stiffness matrix form-finding method is as follows:

1. Assign the topology of the structure, the natural length of the members l_k^0 and the axial stiffness of the component g_k. As specific constraints for the

transition structure, the coordinates of the docking nodes $\mathbf{p}^0_{\text{docking}}$ and boundary nodes $\mathbf{p}^0_{\text{boundary}}$ are predefined so only the initial random positions of the free nodes $\mathbf{p}^0_{\text{free}}$ are given (Figure 6). Calculate the initial strain energy U^0, the stiffness matrix $\mathbf{K}^0$ and the tensions t^0 and force density q^0 of each member. The superscript 0 denotes the 0-th iteration step.

2. Select all DOFs corresponding to the boundary nodes to be fixed and divide the connectivity matrix into $\mathbf{C}_{\text{free}}$ and $\mathbf{C}_{\text{fix}}$. The equilibrium matrix can then be formulated and the unbalanced forces $\mathbf{u}^N$ are derived by equilibrium.

3. Modify the stiffness matrix $\mathbf{K}$ into $\bar{\mathbf{K}}$ and the unbalanced forces $\mathbf{u}^N$ into $\bar{\mathbf{u}}^N$ by fixed nodes constraints. Here, one crucial step to adapt the SMFF method is that the calculation of unbalanced force after constraining the fixing DOFs $\bar{\mathbf{u}}^N$ at the N-th iteration varies between nodal types:

$$\bar{\mathbf{u}}^N = \begin{cases} -(\mathbf{A}_{\text{free}}\mathbf{t}^N - \mathbf{f}_{\text{docking}}) & \text{for docking nodes} \\ -(\mathbf{A}_{\text{free}}\mathbf{t}^N) & \text{for free nodes} \\ \mathbf{0} & \text{for boundary nodes} \end{cases} \tag{35}$$

   Examine the positive definiteness of the stiffness matrix $\bar{\mathbf{K}}$. If the matrix is not positive definite, manually modify it to become $\tilde{\mathbf{K}}$.

4. Calculate the increment of the displacement of the DOFs related to the free nodes:

$$\Delta\mathbf{P}^N = (\tilde{\mathbf{K}}^{N-1})^{-1}\,\bar{\mathbf{u}}^{N-1}$$

5. Add the increment of the displacement to the previous displacement field

$$\mathbf{P}^N = \mathbf{P}^{N-1} + (\eta^N)\,\Delta\mathbf{P}^N$$

   with η being a constant calculated through the bisection method.

6. Update the coordinates of the docking nodes ($\mathbf{p}_{\text{docking}}$) to be back to their original predefined positions, in order to enforce the nodal coordinates in addition to external forces.

7. Iterate the procedure until the i-th unbalanced force component $\bar{\mathbf{u}}_i$ is lower than or equal to the threshold value u_{th}: $\bar{\mathbf{u}}_i \leq u_{th}$, for $i = 1, 2, \ldots, 3n$.

Results In order to validate the adapted stiffness matrix form-finding method, the result from the ground structure method was first reproduced. The output topology and member parameters (stiffness and rest length) were taken from the ground structure results, but random nodal coordinates were given to the free nodes. As illustrated in Figure 6, the same tensegrity configuration is retrieved.

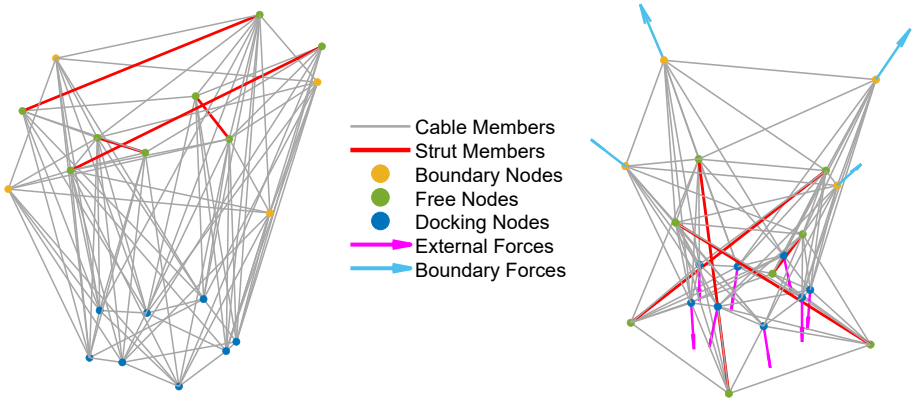

Figure 6: The adapted stiffness matrix form-finding method provides an alternative approach to designing a transition structure. During form-finding both coordinates and residual forces are simultaneously specified at the docking nodes. (a): Initial configuration for the adapted stiffness form-finding method, using the topology found using the ground-structure approach; the coordinates of the free nodes are randomly assigned. (b): Final configuration reproduces the transition structure found previously using topology optimization.

An alternative transition structure designed using the adapted stiffness matrix form-finding method is shown in Figure 7. It has fewer free nodes and a corresponding reduction in number of members ($m_t = 60$). This transition structure could be integrated with the identical tessellated tubular tensegrity tower structure illustrated in Figure 4. Both solutions guarantee the equilibrium of the final assembly and maintain the whole tensegrity assembly to be a Class-I tensegrity structure.

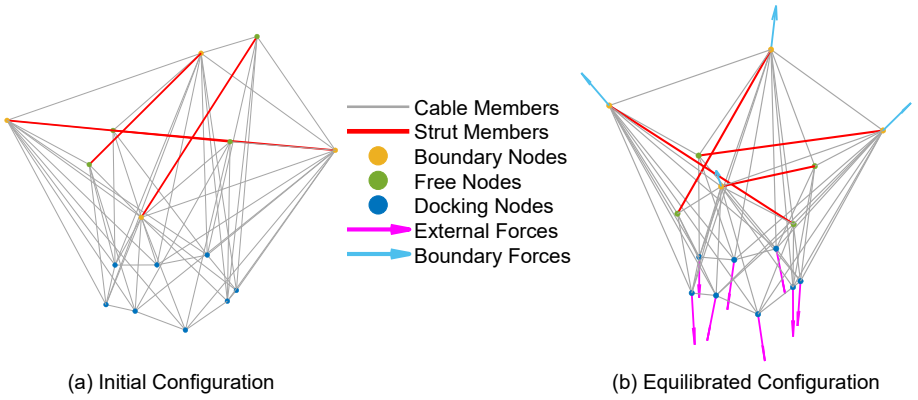

Figure 7: A new solution for the transition structure provided by the adapted stiffness matrix form-finding method. (a): Initial configuration with a reduced number of free nodes and struts connected to boundary nodes. (b): Final configuration of transition structure.

5 Results

5.1 Tessellated Tensegrity Tower Assembly

The resulting configuration for the case study of a *T4* tessellated tensegrity tower assembly is shown in Figure 4 and Table 5, where m_s and m_c are number of strut members and cable members respectively. Note that the assembly consist of 2 transition structures and 1 tessellated tubular tensegrity section, so 16 docking nodes in the tessellated tubular tensegrity will be merged with the docking nodes in the transition structures, leading to the overall 80 nodes in the overall final assembly. From the eigenvalue analysis of the stiffness $\mathbf{K}$ and stress matrices $\mathbf{D}_{\text{free}}$ of the *T4* tessellated tensegrity assembly with end caps, one can conclude that both matrices are positive-definite. The dimension of equilibrium matrix $\mathbf{A} \in \Re^{216\times 328}$ and the rank of equilibrium matrix $\mathbf{A}$ is 216, which means that there is also no internal mechanism for the assembly.

	Transition Structure	Cylindrical Section	Overall Assembly
n	20	56	80
n_{fix}	4	-	8
n_{dock}	8	16	16
m	96	136	328
m_s	4	24	32
m_c	92	112	296

Table 5: The result of *T4* tessellated tensegrity towers assembly

As additional case studies, results for *T3* and *T5* tessellated tensegrity towers with transition structures designed using the ground structure method are shown in Figure 8. Both *T3* and *T5* tessellated tensegrity tower assembly are Class-I tensegrity structures, with symmetry and translational constraints being imposed. The stiffness and stress matrices of the free nodes are verified to be positive-definite, showing that the configurations are stable.

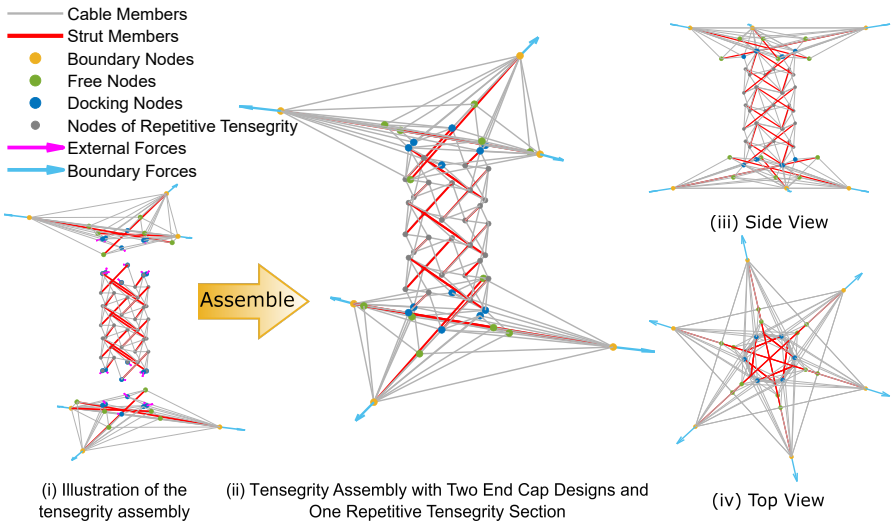

(a) *T3* tessellated tensegrity tower

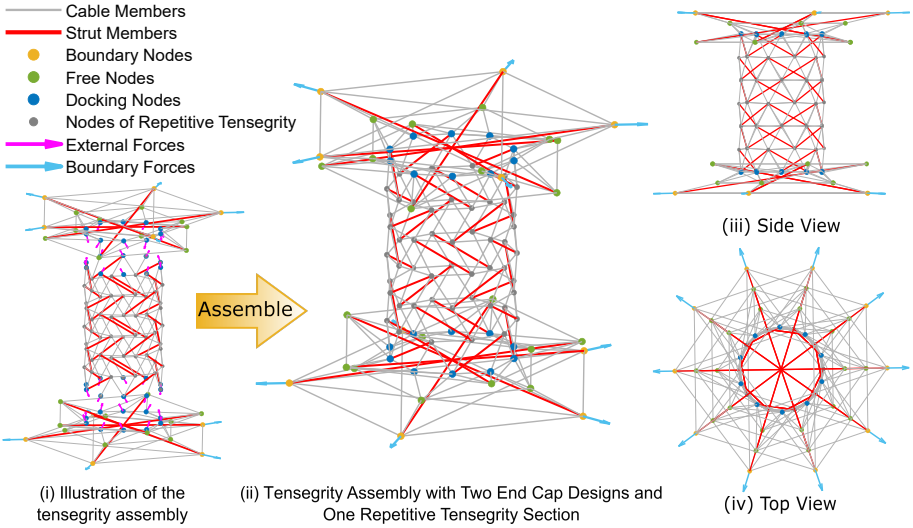

(b) *T5* tessellated tensegrity tower

Figure 8: Tessellated tensegrity structures with corresponding transition structures. (i): Transition structure designs for a repetitive tensegrity tower. (ii): Overview of the assembly where the repetitive tensegrity tower is balanced by the transition structures designs on the top and bottom. (iii/iv): side and top view of the assembly.

5.2 Tessellated Tensegrity Plate Assembly

The adapted stiffness form-finding method form-finding methodology outlined in Section 3 is not restricted to translational symmetry along a single axis. By means of illustration, a tensegrity plate structure is designed by tessellating a repetitive tensegrity unit along two in-plane directions; see Figure 9. The corresponding boundary structures at each side of the plate are designed using the ground structure method.

The elegance of a single repeating unit cell in the tensegrity plate is unfortunately seen to be countered by the complexity of the boundary transition structure. The periodicity of tessellated units does not lead to a symmetric (or periodic) design space for the transition structures; this means that the transition structure on each of the four sides of the tensegrity structure may be different. In order to find a solution, the Class-I constraint had to be relaxed as it prohibitively reduced the design space: no initial nodal configurations could be found that yielded acceptable solutions for the transition structure. Instead, the option of a Class-II transition structure enabled comparatively elegant solutions, such as the rotationally symmetric configurations shown in Figure 9. Thus, the overall assembly of the tessellated tensegrity plate is a Class-II tensegrity structure. Both the stiffness and the stress matrices associated with the free nodes are positive-definite, and the structure is therefore stable.

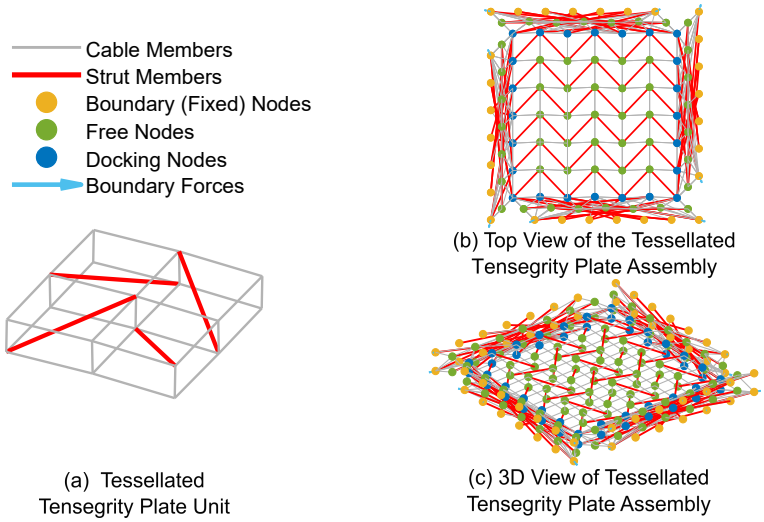

Figure 9: Design of a flat tessellated tensegrity plate in a 2D tessellation. (a): Tessellated tensegrity plate unit. The plate structure in the middle of the assembly is formed by the tessellation of the unit. (b/c): Top view and 3D view of the tessellated tensegrity plate.

6 Discussion

An important contribution of this paper is to provide a tensegrity form-finding method that has the ability to specify both coordinates and external loads at certain nodes, but is not subject to the limitations of ground structure methods. Applications might include tensegrity structures which must interface with another structure that transfers a load, such as a column supporting a roof or the transition structures that balance the tessellated tensegrity structures in this work. Further, as periodic structures possess many novel and interesting physical properties [49, 50], the proposed tubular tessellated tensegrity structures have potential to be used in applications for wave propagation, noise reduction or spring-like components in dampers. It is noted that the structures designed with the current methodology are not necessarily self-equilibrated, which may preclude certain applications.

The proposed adapted stiffness matrix form-finding method is capable of providing solutions for cases where coordinates and loads are prescribed at specific nodes, but also incorporates symmetry (rotational and translational) constraints as well as Class-I tensegrity conditions. This opens up the ability to design truly repetitive tensegrity structures (topology, geometry and prestress), whilst providing a richer design space and tensegrities with fewer members than ground structure methods where the coordinates of all nodes are fixed. The adapted SMFF methods have been applied to design tessellated tensegrity structures with identical repetitive units, and transition structures that balance the forces and connect to a fixed boundary.

The proposed form-finding method shares similar limitations to existing stiffness-matrix form-finding methods. Although physical material properties are specified *a priori*, the resulting designs might carry loads that could result in material failure or member buckling. This means that the selection of desired level of prestress and physical sizing of members must be performed separately after the form-finding stage. Further, specifying a suitable initial topology (*i.e.* member connectivity and cable/strut assignment) remains an open challenge. For instance, the transition structures for the tessellated tensegrity plate presented in this work are overly complex in comparison;

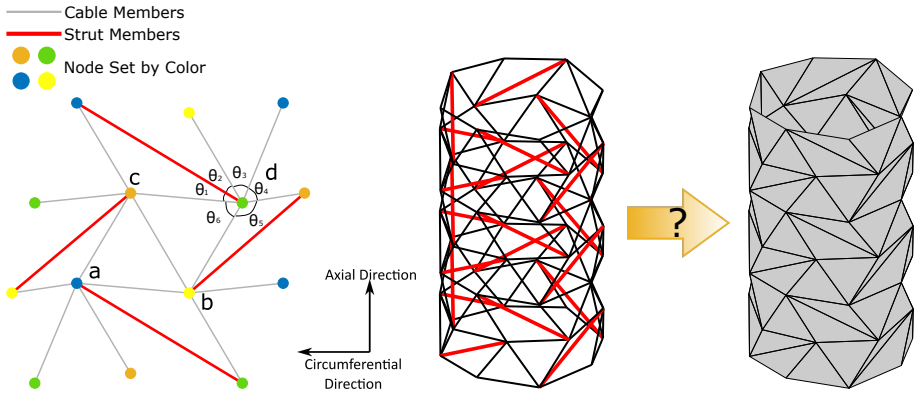

Figure 10: (a) For any node inside a tubular tensegrity structure, the total angle is the sum of sector angles θ_i, where $n = 6$. (b) For tessellated tensegrity structures where nodal angles sum to 2π, there exists a cylindrical origami dual.

in turn, this negates some of the benefits of a tessellated tensegrity structure.

In this work, the tessellation boundary conditions have been limited to tubular and planar tensegrity structures. The primary challenge in designing a 3D tessellation would be finding the topology of the tessellated unit cell, either as direct input into the adapted stiffness matrix form-finding method, or by specifying suitable nodal coordinates for the ground structure methods. One approach (as used in this work for the tubular transition structure) could be to use the ground structure method for an initial design, which is then simplified using the adapted stiffness matrix form-finding method. Alternatively, 2D tessellated planes could be stacked to create a 3D volume, although this would result in a Class-II tensegrity structure.

Lastly, and fascinatingly, during the design of the tubular tessellated tensegrity it was found that configurations exist where the sum of the member angles around a node adds up to 2π, as illustrated in Figure 10. This suggests that the tessellated tensegrity tubular configuration may have an origami dual, as previously discussed by Tachi [51].

7 Conclusions

In this paper, we have proposed an adapted stiffness matrix form-finding method with symmetry, translational and Class-I constraints to design tessellated tensegrity towers and a tensegrity plate structure. These tessellated structures are repetitive not only in their topology, but also geometry and self-stress; this offers the opportunity to design large-scale tensegrity structures with repeating units.

However, as each tessellated unit cell relies on its adjacent members for equilibrium, the resulting tessellation is not in global equilibrium. In order to attach the structure to a fixed boundary, transition structures must therefore be designed. The form-finding challenge presented by simultaneously prescribing external loads and nodal coordinates at the attachment points with the tessellated tensegrity structure was resolved using two approaches. First, a ground structure method was extended with both symmetric and Class-I constraints to form overall Class-I tessellated tensegrity tower assemblies. Next, the stiffness matrix form-finding method was adapted to account for external loads and boundary conditions, which enables finding transition structures for a given tensegrity topology.

The adapted stiffness matrix form-finding methods not only enable the design of repetitive tensegrity structures, but also facilitate the design of tensegrity structures that are designed to carry external loads at specific interface points to external structures (*e.g.* in structural engineering applications). Avenues for future work include analyzing the mechanical responses of the tensegrity assemblies under external loads, as well as extending the methodology to 3D tessellations.

8 Acknowledgement

Funding: This work was supported by the China Scholarship Council and University of Bristol joint PhD programme. The authors also wish to thank the reviewers for all comments and suggestions received.

References

[1] Zacharias Vangelatos, Andrea Micheletti, Costas P Grigoropoulos, and Fernando Fraternali. Design and testing of bistable lattices with tensegrity architecture and nanoscale features fabricated by multiphoton lithography. *Nanomaterials*, 10(4):652, 2020.

[2] Feng Fu. Structural behavior and design methods of tensegrity domes. *Journal of Constructional Steel Research*, 61(1):23–35, 2005.

[3] G Carpentieri and RE Skelton. On the dynamics of tensegrity bridges. *J. Aerosp. Eng. Mech.*, 1(1):48–62, 2017.

[4] Yao Chen, Jiayi Yan, and Jian Feng. Nonlinear form-finding of symmetric cable–strut structures using stiffness submatrices associated with full symmetry subspace. *Archive of Applied Mechanics*, 90(8):1783–1794, 2020.

[5] Landolf Rhode-Barbarigos, Nizar Bel Hadj Ali, René Motro, and Ian FC Smith. Designing tensegrity modules for pedestrian bridges. *Engineering Structures*, 32(4):1158–1167, 2010.

[6] JY Zhang, M Ohsaki, and Y Kanno. A direct approach to design of geometry and forces of tensegrity systems. *International Journal of Solids and Structures*, 43(7-8):2260–2278, 2006.

[7] M Ohsaki and Y Kanno. Form-finding of cable domes with specified stresses by using nonlinear programming. *Proceedings of IASS-APCS*, 2003.

[8] AG Tibert and Sergio Pellegrino. Review of form-finding methods for tensegrity structures. *International Journal of Space Structures*, 18(4):209–223, 2003.

[9] K Koohestani and SD Guest. A new approach to the analytical and numerical form-finding of tensegrity structures. *International Journal of Solids and Structures*, 50(19):2995–3007, 2013.

[10] Mariano Modano, Ida Mascolo, Fernando Fraternali, and Zbigniew Bieniek. Numerical and analytical approaches to the self-equilibrium problem of class $\theta = 1$ tensegrity metamaterials. *Frontiers in materials*, 5:5, 2018.

[11] Reg Connelly and Maria Terrell. Globally rigid symmetric tensegrities. *Structural Topology 1995 núm 21*, 1995.

[12] Li-Yuan Zhang, Yue Li, Yan-Ping Cao, Xi-Qiao Feng, and Huajian Gao. Self-equilibrium and super-stability of truncated regular polyhedral tensegrity structures: a unified analytical solution. *Proceedings of the Royal Society A: Mathematical, Physical and Engineering Sciences*, 468(2147):3323–3347, 2012.

[13] Li-Yuan Zhang, Yue Li, Yan-Ping Cao, and Xi-Qiao Feng. A unified solution for self-equilibrium and super-stability of rhombic truncated regular polyhedral tensegrities. *International Journal of Solids and Structures*, 50(1):234–245, 2013.

[14] Li-Yuan Zhang, Shi-Xin Zhu, Song-Xue Li, and Guang-Kui Xu. Analytical form-finding of tensegrities using determinant of force-density matrix. *Composite Structures*, 189:87–98, 2018.

[15] Cornel Sultan, Martin Corless, and Robert E Skelton. The prestressability problem of tensegrity structures: some analytical solutions. *International Journal of Solids and Structures*, 38(30-31):5223–5252, 2001.

[16] Yue Li, Xi-Qiao Feng, Yan-Ping Cao, and Huajian Gao. Constructing tensegrity structures from one-bar elementary cells. *Proceedings of the Royal Society A: Mathematical, Physical and Engineering Sciences*, 466(2113):45–61, 2010.

[17] Yao Chen, Qiuzhi Sun, and Jian Feng. Improved form-finding of tensegrity structures using blocks of symmetry-adapted force density matrix. *Journal of Structural Engineering*, 144(10):04018174, 2018.

[18] G Gomez Estrada, H-J Bungartz, and Camilla Mohrdieck. Numerical form-finding of tensegrity structures. *International Journal of Solids and Structures*, 43(22-23):6855–6868, 2006.

[19] Hoang Chi Tran and Jaehong Lee. Advanced form-finding of tensegrity structures. *Computers & structures*, 88(3-4):237–246, 2010.

[20] Xing-Fei Yuan, Shuo Ma, and Shu-Hui Jiang. Form-finding of tensegrity structures based on the levenberg–marquardt method. *Computers & Structures*, 192:171–180, 2017.

[21] Jianguo Cai, Xinyu Wang, Xiaowei Deng, and Jian Feng. Form-finding method for multi-mode tensegrity structures using extended force density method by grouping elements. *Composite Structures*, 187:1–9, 2018.

[22] K Koohestani. Innovative numerical form-finding of tensegrity structures. *International Journal of Solids and Structures*, 206:304–313, 2020.

[23] Sergio Pellegrino. *Mechanics of kinematically indeterminate structures*. PhD thesis, University of Cambridge, 1986.

[24] Andrea Micheletti and William Williams. A marching procedure for form-finding for tensegrity structures. *Journal of mechanics of materials and structures*, 2(5):857–882, 2007.

[25] Vinicius Arcaro and Hojjat Adeli. Form-finding and analysis of hyperelastic tensegrity structures using unconstrained nonlinear programming. *Engineering Structures*, 191:439–446, 2019.

[26] Michael R Barnes. Form finding and analysis of tension structures by dynamic relaxation. *International journal of space structures*, 14(2):89–104, 1999.

[27] H-J Schek. The force density method for form finding and computation of general networks. *Computer methods in applied mechanics and engineering*, 3(1):115–134, 1974.

[28] Li-Yuan Zhang, Yue Li, Yan-Ping Cao, and Xi-Qiao Feng. Stiffness matrix based form-finding method of tensegrity structures. *Engineering structures*, 58:36–48, 2014.

[29] Shintaro Ehara and Yoshihiro Kanno. Topology design of tensegrity structures via mixed integer programming. *International Journal of Solids and Structures*, 47(5):571–579, 2010.

[30] Yoshihiro Kanno. Exploring new tensegrity structures via mixed integer programming. *Structural and Multidisciplinary Optimization*, 48(1):95–114, 2013.

[31] Yoshihiro Kanno. Topology optimization of tensegrity structures under compliance constraint: a mixed integer linear programming approach. *Optimization and Engineering*, 14(1):61–96, 2013.

[32] KIU Nanayakkara, Linwei He, Helen E Fairclough, and Matthew Gilbert. A simple layout optimization formulation for load-carrying tensegrity structures. *Structural and Multidisciplinary Optimization*, pages 1–15, 2020.

[33] Ke Liu and Glaucio H Paulino. Tensegrity topology optimization by force maximization on arbitrary ground structures. *Structural and Multidisciplinary Optimization*, 59(6):2041–2062, 2019.

[34] Ke Liu, Tomás Zegard, Phanisri P Pratapa, and Glaucio H Paulino. Unraveling tensegrity tessellations for metamaterials with tunable stiffness and bandgaps. *Journal of the Mechanics and Physics of Solids*, 131:147–166, 2019.

[35] Li-Yuan Zhang, Song-Xue Li, Shi-Xin Zhu, Bo-Yang Zhang, and Guang-Kui Xu. Automatically assembled large-scale tensegrities by truncated regular polyhedral and prismatic elementary cells. *Composite Structures*, 184:30–40, 2018.

[36] John L Rohmer, Edwin A Peraza Hernandez, Robert E Skelton, Darren J Hartl, and Dimitris C Lagoudas. An experimental and numerical study of shape memory alloy-based tensegrity/origami structures. In *ASME 2015 international mechanical engineering congress and exposition*. American Society of Mechanical Engineers Digital Collection, 2015.

[37] Yue Li, Xi-Qiao Feng, Yan-Ping Cao, and Huajian Gao. A monte carlo form-finding method for large scale regular and irregular tensegrity structures. *International Journal of Solids and Structures*, 47(14-15):1888–1898, 2010.

[38] Milenko Masic, Robert E Skelton, and Philip E Gill. Algebraic tensegrity form-finding. *International Journal of Solids and Structures*, 42(16-17):4833–4858, 2005.

[39] Hoang Chi Tran and Jaehong Lee. Initial self-stress design of tensegrity grid structures. *Computers & structures*, 88(9-10):558–566, 2010.

[40] Hoang Chi Tran and Jaehong Lee. Self-stress design of tensegrity grid structures with exostresses. *International Journal of Solids and Structures*, 47(20):2660–2671, 2010.

[41] Li-Yuan Zhang, Hong-Ping Zhao, and Xi-Qiao Feng. Constructing large-scale tensegrity structures with bar–bar connection using prismatic elementary cells. *Archive of Applied Mechanics*, 85(3):383–394, 2015.

[42] Rene Motro. *Tensegrity: structural systems for the future*. Elsevier, 2003.

[43] Heping Liu, Jinsong Geng, and Ani Luo. Tensegrity configuration method for connecting tensegrity units along their axes. *Composite Structures*, 162:341–350, 2017.

[44] Simon Guest. The stiffness of prestressed frameworks: a unifying approach. *International Journal of Solids and Structures*, 43(3-4):842–854, 2006.

[45] Makoto Ohsaki and Jingyao Zhang. Stability conditions of prestressed pin-jointed structures. *International Journal of Non-Linear Mechanics*, 41(10):1109–1117, 2006.

[46] Hidenori Murakami. Static and dynamic analyses of tensegrity structures. part ii. quasi-static analysis. *International Journal of Solids and Structures*, 38(20):3615–3629, 2001.

[47] MATLAB. *9.7.0.1190202 (R2019b)*. The MathWorks Inc., Natick, Massachusetts, 2018.

[48] Cornel Sultan, Martin Corless, and Robert E Skelton. Symmetrical reconfiguration of tensegrity structures. *International Journal of Solids and Structures*, 39(8):2215–2234, 2002.

[49] F Fabbrocino and G Carpentieri. Three-dimensional modeling of the wave dynamics of tensegrity lattices. *Composite Structures*, 173:9–16, 2017.

[50] Li-Yuan Zhang, Xu Yin, Jiang Yang, Ao Li, and Guang-Kui Xu. Multilevel structural defects-induced elastic wave tunability and localization of a tensegrity metamaterial. *Composites Science and Technology*, 207:108740, 2021.

[51] Tomohiro Tachi. Design of infinitesimally and finitely flexible origami based on reciprocal figures. *J. Geom. Graph*, 16(2):223–234, 2012.

A Appendix

A.1 Connectivity Matrix of Calculation Model

The connectivity matrix of calculation model of the tessellated tensegrity structure $\mathbf{C} \in \Re^{19\times 14}$ is first expressed:

$$\mathbf{C} = \begin{pmatrix}
1 & 0 & 0 & 0 & -1 & 0 & 0 & 0 & 0 & 0 & 0 & 0 & 0 & 0 \\
1 & 0 & 0 & 0 & 0 & -1 & 0 & 0 & 0 & 0 & 0 & 0 & 0 & 0 \\
0 & 1 & 0 & 0 & 0 & 0 & -1 & 0 & 0 & 0 & 0 & 0 & 0 & 0 \\
1 & 0 & 0 & 0 & 0 & 0 & 0 & 0 & 0 & 0 & 0 & 0 & 0 & -1 \\
1 & -1 & 0 & 0 & 0 & 0 & 0 & 0 & 0 & 0 & 0 & 0 & 0 & 0 \\
0 & 1 & 0 & 0 & 0 & 0 & 0 & -1 & 0 & 0 & 0 & 0 & 0 & 0 \\
1 & 0 & -1 & 0 & 0 & 0 & 0 & 0 & 0 & 0 & 0 & 0 & 0 & 0 \\
0 & 1 & -1 & 0 & 0 & 0 & 0 & 0 & 0 & 0 & 0 & 0 & 0 & 0 \\
0 & 1 & 0 & -1 & 0 & 0 & 0 & 0 & 0 & 0 & 0 & 0 & 0 & 0 \\
0 & 0 & 1 & 0 & 0 & 0 & 0 & 0 & 0 & 0 & 0 & 0 & -1 & 0 \\
0 & 0 & 1 & -1 & 0 & 0 & 0 & 0 & 0 & 0 & 0 & 0 & 0 & 0 \\
0 & 0 & 0 & 1 & 0 & 0 & 0 & 0 & -1 & 0 & 0 & 0 & 0 & 0 \\
0 & 0 & 1 & 0 & 0 & 0 & 0 & 0 & 0 & 0 & 0 & -1 & 0 & 0 \\
0 & 0 & 0 & 1 & 0 & 0 & 0 & 0 & 0 & 0 & -1 & 0 & 0 & 0 \\
0 & 0 & 0 & 1 & 0 & 0 & 0 & 0 & 0 & -1 & 0 & 0 & 0 & 0 \\
1 & 0 & 0 & 0 & 0 & 0 & -1 & 0 & 0 & 0 & 0 & 0 & 0 & 0 \\
0 & 0 & 1 & 0 & 0 & 0 & 0 & 0 & 0 & 0 & 0 & 0 & 0 & -1 \\
0 & 1 & 0 & 0 & 0 & 0 & 0 & 0 & -1 & 0 & 0 & 0 & 0 & 0 \\
0 & 0 & 0 & 1 & 0 & 0 & 0 & 0 & 0 & 0 & 0 & -1 & 0 & 0
\end{pmatrix}$$